Influence of coherence length, signal-to-noise ratio, log transform, and low-pass filtering on layer thickness assessment with OCT in the retina

Jansonius, Nomdo M.; Cervantes, Joel; Reddikumar, Maddipatla; Cense, Barry

Published in:
Biomedical optics express

DOI:
10.1364/BOE.7.004490

Publication date:
2016

Research Article | Vol. 7, No. 11 | 1 Nov 2016 | BIOMEDICAL OPTICS EXPRESS 4490

Biomedical Optics EXPRESS

Influence of coherence length, signal-to-noise ratio, log transform, and low-pass filtering on layer thickness assessment with OCT in the retina

NOMDO M. JANSONIUS,[1,*] JOEL CERVANTES,[2] MADDIPATLA REDDIKUMAR,[2] AND BARRY CENSE[2]

[1]*Department of Ophthalmology, University of Groningen, University Medical Center Groningen, Groningen, The Netherlands*
[2]*Center for Optical Research and Education, Utsunomiya University, Utsunomiya, Tochigi, Japan*
[*]*n.m.jansonius@umcg.nl*

Abstract: Optical coherence tomography (OCT) images of the retina are inevitably affected by the finite width of the coherence function and noise. To make low-reflective layers visible, the raw OCT signal is log transformed; to reduce the effect of noise the images can be low-pass filtered. We determined the effects of these operations on layer thickness assessment, as a function of signal-to-noise ratio (SNR), by performing measurements in a phantom eye and modeling. The log transform appeared to be the key factor in a SNR-dependent overestimation of peak widths and a less predictive bias in the widths of low-reflective layers.

OCIS codes: (100.0100) Image processing; (100.3008) Image recognition, algorithms and filters; (110.0113) Imaging through turbid media; (110.4500) Optical coherence tomography; (170.4460) Ophthalmic optics and devices; (170.4470) Ophthalmology.

References and links

1. R. de Kinkelder, D. M. de Bruin, F. D. Verbraak, T. G. van Leeuwen, and D. J. Faber, "Comparison of retinal nerve fiber layer thickness measurements by spectral-domain optical coherence tomography systems using a phantom eye model," J. Biophotonics **6**(4), 314–320 (2013).
2. S. Darma, P. H. Kok, T. J. van den Berg, M. D. Abràmoff, D. J. Faber, C. A. Hulsman, F. Zantvoord, M. P. Mourits, R. O. Schlingemann, and F. D. Verbraak, "Optical density filters modeling media opacities cause decreased SD-OCT retinal layer thickness measurements with inter- and intra-individual variation," Acta Ophthalmol. **93**(4), 355–361 (2015).
3. D. W. Lee, J. M. Kim, K. H. Park, C. Y. Choi, and J. G. Cho, "Effect of media opacity on retinal nerve fiber layer thickness measurements by optical coherence tomography," J. Ophthalmic Vis. Res. **5**(3), 151–157 (2010).
4. J. C. Mwanza, A. M. Bhorade, N. Sekhon, J. J. McSoley, S. H. Yoo, W. J. Feuer, and D. L. Budenz, "Effect of cataract and its removal on signal strength and peripapillary retinal nerve fiber layer optical coherence tomography measurements," J. Glaucoma **20**(1), 37–43 (2011).
5. Y. Nakatani, T. Higashide, S. Ohkubo, H. Takeda, and K. Sugiyama, "Effect of cataract and its removal on ganglion cell complex thickness and peripapillary retinal nerve fiber layer thickness measurements by fourier-domain optical coherence tomography," J. Glaucoma **22**(6), 447–455 (2013).
6. D. Marr and E. Hildreth, "Theory of edge detection," Proc. R. Soc. Lond. B Biol. Sci. **207**(1167), 187–217 (1980).
7. R. J. Watt, *Visual Processing* (Lawrence Earlbaurn Associates, 1988).
8. D. C. DeBuc, *A Review of Algorithms for Segmentation of Retinal Image Data Using Optical Coherence Tomography* (INTECH Open Access Publisher, 2011).
9. N. M. Jansonius, L. Stam, T. de Jong, and B. A. Pijpker, "Quantitative analysis of illusory movement: spatial filtering and line localization in the human visual system," Perception **43**(12), 1329–1340 (2014).
10. F. G. Junoy Montolio, W. Meems, M. S. Janssens, L. Stam, and N. M. Jansonius, "Lateral inhibition in the human visual system in patients with glaucoma and healthy subjects: a case-control study," PLoS One **11**(3), e0151006 (2016).
11. F. M. Gladys, M. Matsuda, Y. Lim, B. J. Jackin, T. Imai, Y. Otani, T. Yatagai, and B. Cense, "Developmental and morphological studies in Japanese medaka with ultra-high resolution optical coherence tomography," Biomed. Opt. Express **6**(2), 297–308 (2015).

#273230 http://dx.doi.org/10.1364/BOE.7.004490
Journal © 2016 Received 4 Aug 2016; revised 3 Oct 2016; accepted 3 Oct 2016; published 7 Oct 2016

Biomedical Optics EXPRESS

12. D. M. de Bruin, R. H. Bremmer, V. M. Kodach, R. de Kinkelder, J. van Marle, T. G. van Leeuwen, and D. J. Faber, "Optical phantoms of varying geometry based on thin building blocks with controlled optical properties," J. Biomed. Opt. **15**(2), 025001 (2010).
13. B. Cense, *Optical Coherence Tomography for Retinal Imaging* (PhD thesis, University of Twente, 2005).
14. N. Nassif, B. Cense, B. Park, M. Pierce, S. Yun, B. Bouma, G. Tearney, T. Chen, and J. de Boer, "In vivo high-resolution video-rate spectral-domain optical coherence tomography of the human retina and optic nerve," Opt. Express **12**(3), 367–376 (2004).
15. A. F. Fercher, W. Drexler, C. K. Hitzenberger, and T. Lasser, "Optical coherence tomography - principles and applications," Rep. Prog. Phys. **66**(2), 239–303 (2003).
16. H. Ishikawa, D. M. Stein, G. Wollstein, S. Beaton, J. G. Fujimoto, and J. S. Schuman, "Macular segmentation with optical coherence tomography," Invest. Ophthalmol. Vis. Sci. **46**(6), 2012–2017 (2005).
17. T. C. Chen, B. Cense, J. W. Miller, P. A. D. Rubin, D. G. Deschler, E. S. Gragoudas, and J. F. de Boer, "Histologic correlation of in vivo optical coherence tomography images of the human retina," Am. J. Ophthalmol. **141**(6), 1165–1168 (2006).
18. M. V. Srinivasan, S. B. Laughlin, and A. Dubs, "Predictive coding: a fresh view of inhibition in the retina," Proc. R. Soc. Lond. B Biol. Sci. **216**(1205), 427–459 (1982).
19. J. H. van Hateren, "A theory of maximizing sensory information," Biol. Cybern. **68**(1), 23–29 (1992).
20. M. K. Garvin, M. D. Abràmoff, X. Wu, S. R. Russell, T. L. Burns, and M. Sonka, "Automated 3-D intraretinal layer segmentation of macular spectral-domain optical coherence tomography images," IEEE Trans. Med. Imaging **28**(9), 1436–1447 (2009).
21. S. J. Chiu, X. T. Li, P. Nicholas, C. A. Toth, J. A. Izatt, and S. Farsiu, "Automatic segmentation of seven retinal layers in SDOCT images congruent with expert manual segmentation," Opt. Express **18**(18), 19413–19428 (2010).
22. H. Springelkamp, K. Lee, R. C. Wolfs, G. H. Buitendijk, W. D. Ramdas, A. Hofman, J. R. Vingerling, C. C. Klaver, M. D. Abràmoff, and N. M. Jansonius, "Population-based evaluation of retinal nerve fiber layer, retinal ganglion cell layer, and inner plexiform layer as a diagnostic tool for glaucoma," Invest. Ophthalmol. Vis. Sci. **55**(12), 8428–8438 (2014).
23. N. O'Leary, P. H. Artes, D. M. Hutchison, M. T. Nicolela, and B. C. Chauhan, "Rates of retinal nerve fibre layer thickness change in glaucoma patients and control subjects," Eye (Lond.) **26**(12), 1554–1562 (2012).
24. C. K. Leung, M. Yu, R. N. Weinreb, G. Lai, G. Xu, and D. S. Lam, "Retinal nerve fiber layer imaging with spectral-domain optical coherence tomography: patterns of retinal nerve fiber layer progression," Ophthalmology **119**(9), 1858–1866 (2012).
25. J. R. Vianna, V. M. Danthurebandara, G. P. Sharpe, D. M. Hutchison, A. C. Belliveau, L. M. Shuba, M. T. Nicolela, and B. C. Chauhan, "Importance of normal aging in estimating the rate of glaucomatous neuroretinal rim and retinal nerve fiber layer loss," Ophthalmology **122**(12), 2392–2398 (2015).
26. G. Holló and Q. Zhou, "Evaluation of retinal nerve fiber layer thickness and ganglion cell complex progression rates in healthy, ocular hypertensive, and glaucoma eyes with the Avanti RTVue-XR optical coherence tomograph based on 5-year follow-up," J. Glaucoma (to be published).

1. Introduction

Optical coherence tomography (OCT) is a popular method for imaging of the human retina, and for quantification of retinal layer thicknesses. Changes in the thickness of a retinal layer of a patient as a function of time may be used for the diagnosis and management of retinal diseases and glaucoma. Recent measurements on a phantom model retina have demonstrated that the layer thicknesses that are assessed with various OCT instruments are not correct [1]. Moreover, layer thicknesses depend on the signal-to-noise ratio (SNR) [2] and change after cataract extraction [3–5].

The raw signal that is detected in spectral-domain (SD) OCT is the result of interference between light returning from the sample and reference arm of an interferometer. This signal is then mapped to k-space and Fourier transformed to z-space, where the reflected intensity is shown as a function of depth. OCT is based on low coherence interferometry, and the broadband light sources that are used in OCT have a coherence length of several μm. Reflections are convolved with the coherence function, and owing to the finite width of the coherence function this leads to low-pass filtering of the signal in z-space. Furthermore, for display purposes the signal is log transformed to reduce contrast and thus improve the visibility of the various retinal layers. Figure 1 illustrates this transform.

Biomedical Optics EXPRESS

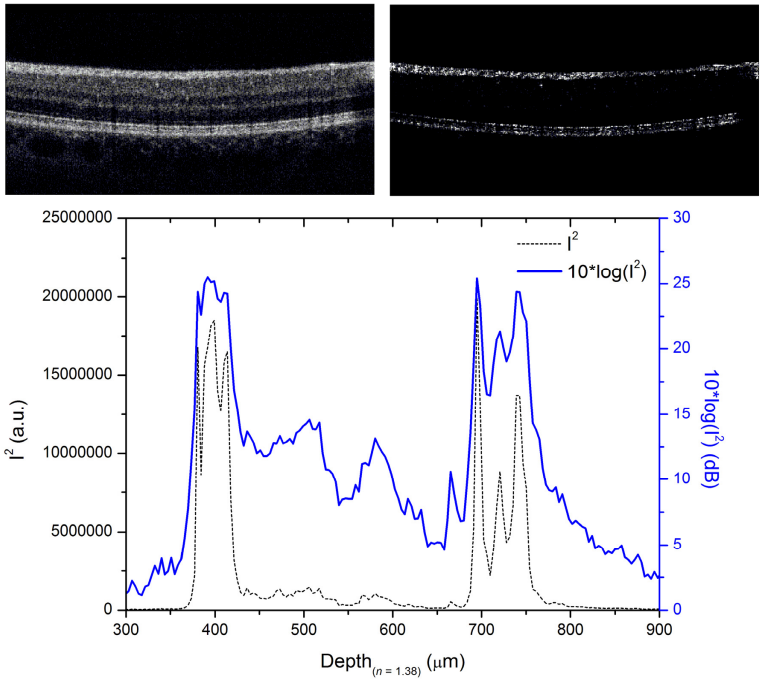

Fig. 1. Upper panel, left: B-scan of a 15° wide horizontal scan taken at 7.5° eccentricity above the fovea. The image consists of 1000 A-scans. The image of the intensity (I^2) is logarithmically scaled and displayed in grayscale (8 bit, 256 gray values) over 35 dB above the noise floor. Upper panel, right: The same data scaled linearly over 256 gray values, while saturating the top 90% gray values to white. Even though heavy saturation is used, the layers between the RNFL and the photoreceptors/RPE remain invisible, demonstrating why B-scans are usually logarithmically scaled. Lower panel: The intensity (black) and its logarithmic counterpart (blue) both shown as a function of depth, averaged over the central 100 A-scans of the images in the upper panel.

The borders between the various retinal layers may be considered edges. The position of an edge is not affected by low-pass filtering (if depicted by, e.g., the zero-crossing of the second derivative of the filtered intensity pattern [6]; Fig. 2, left panel), but this is no longer the case if (1) there are other edges within the range of the filter (layer thickness not small compared to coherence length [7]; or (2) the output of the filter is transformed. A log transform causes a spurious shift of the edge towards the side with the lower intensity (Fig. 2, middle panel).

The log-transformed output as a function of depth is called the A-scan, and a series of A-scans together form a B-scan. For the segmentation of retinal layers, one of the preprocessing steps that is often used before the segmentation is low-pass filtering, at this stage applied intentionally [8]. This filtering might also induce spurious effects. If a narrow intensity peak between two layers with different intensities is low-pass filtered, then its location is apparently shifted towards the side with the higher intensity (Fig. 2, right panel). In psychophysics, this phenomenon is known as illusory movement [9, 10]. Importantly, illusory movement requires a low contrast between peak and flanking areas, and a large contrast between the two flanking areas. Therefore, the phenomenon only affects the A-scan beyond the log transform.

Biomedical Optics EXPRESS

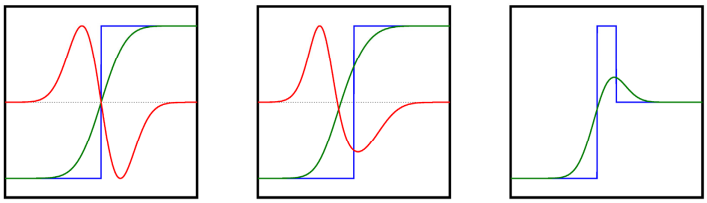

Fig. 2. Left panel: The position of an edge (blue), depicted by the zero-crossing of the second derivative (red), is not affected by low-pass filtering (green). Middle panel: Effect of a log transform on the position of an edge: the transform causes a spurious shift of the edge towards the side with the lower intensity. Right panel: Illustration of illusory movement: the peak of a bright line that is flanked by two fields with different luminances appears to be shifted towards the field with the higher luminance – if low-pass filtered.

The aim of this study was to determine the influence of (1) coherence length and the log transform and (2) low-pass filtering of the A-scan on layer thicknesses as assessed with OCT. For this purpose we (1) performed A-scan measurements using a range of light source powers (SNRs) in a phantom eye with known layer thicknesses, (2) modeled the A-scan for a range of coherence lengths and light source powers, and (3) modeled the effects of low-pass filtering on the positions of the peaks and valleys in the A-scan and the corresponding first derivative.

2. Method

Phantom eye measurements

Measurements were performed with a custom-built SD-OCT system (modified from an earlier built ultra-high resolution SD-OCT system [11]) on a retinal phantom [1, 12]. Light from a superluminescent diode (HP-SLD-371, Superlum) with a center wavelength of 850 nm, an optical bandwidth of 50 nm (full width at half maximum; FWHM), and a coherence length of 6 um in tissue (n = 1.38) [13] was sent through single mode fiber (Corning HI780) through an optical isolator (Thorlabs) and coupled into an 80/20 2x2 fiber coupler (Thorlabs). In the reference arm, a collimator and lens (f30 mm, f60 mm, respectively) and gold-coated mirror (Thorlabs) were used to return light into the interferometer. The mirror in the reference arm was tipped to maintain a detector saturation of approximately 80%. In the sample arm, the light was collimated (f16 mm) and sent through a variable neutral density filter (Thorlabs), so that measurements could be made with different amounts of attenuation. The attenuation was quantified with an Ophir broadband power meter. All previously mentioned lenses were achromatic lenses designed for use with near infra red light (Thorlabs). An XY-galvanometer scanner (Thorlabs) was used for raster scanning. The light was focused onto the sample with an f10 mm microscope objective (Nikon). In the detection arm, the light was collimated with an f75 mm air-spaced achromatic lens optimized for use in the near infra red (Thorlabs), and dispersed with an 1800 lines per mm grating (Wasatch Photonics) at a Littrow angle of approximately 47°. The spectrum was focused onto a line scan camera (Avviva EM4, E2V) with a custom-made lens with a focal length of approximately 180 mm. The camera has 4096 detector elements, each measuring 10 by 10 µm. The fiber tip was imaged onto the detector with a spot size of 19 µm $1/e^2$, measured at 840 nm with a beam profiler (Thorlabs). The relatively high spectral resolution of this spectrometer, of ~50 nm/4096 = ~0.012 nm/pixel resulted in an imaging depth of 4.8 mm in air. Using noise analysis, the efficiency of the spectrometer was quantified, and equal to 19.7% [14]. Based on this efficiency and an input power of 750 µW, the sensitivity of the system was estimated at 102.6 dB. Images were acquired at an acquisition rate of 25 kHz, with an integration time of 36 µs per A-scan, with 1000 A-scans per B-scan. The system was operated in LabVIEW, while the data was post-processed in Matlab.

Biomedical Optics EXPRESS

Images were recorded from a phantom model retina, consisting of several layers of 50 µm thick silicone rubber with different reflectivity (Table 1) [1, 12]. Images were taken such that the layers were oriented perfectly perpendicular with respect to the scanning beam. The central ~800 A-scans of one B-scan were averaged into one depth profile to reduce the influence of speckle noise.

Table 1. Phantom eye layer thickness and reflectivity

Layer number	Thickness (µm)	Reflectivity (a.u.)
1	50	0.0
2	50	0.1
3	50	0.0
4	50	0.1
5	50	0.0
6	50	0.8
7	50	0.0

Modeling the effects of light source power (signal-to-noise ratio) and coherence length on the log transformed output (A-scan)

Reflectivity R (a.u.) as a function of depth z, $R(z)$, was modeled with a resolution of 0.1 µm. Five layers of 50 µm each were employed, with R = 0, 0.1, 0, 0.8, and 0, respectively. The output of the spectrometer was presumed to be proportional to the light source power P and the square root of R [12]. Five different powers were used, being P = 1, 2, 4, 8, and 16 a.u., respectively. The influence of coherence length l_c was modeled by convolving the output of the spectrometer with a Gaussian filter $h(z)$ with standard deviation $\sigma = 0.5 l_c/1.18$ (assuming a Gaussian shape of the coherence function). Three different coherence-length values were used, being l_c = 6, 12, and 24 µm (σ = 2.5, 5, and 10 µm, respectively [15]; the coherence length of modern, clinical SD-OCT devices is typically 6 (Topcon 3D OCT 2000) to 7 (Heidelberg Spectralis) µm in tissue (n = 1.38)). Finally, a log transform was performed to calculate the output as a function of z (the A-scan):

$$A-scan\ (dB) = 20 \cdot \log(h(z) * \sqrt{R(z)} \cdot P + N) \qquad (1)$$

where $h(z)$ is the (Gaussian) coherence function, $R(z)$ the reflectivity, P the light source power, and N the noise, that is, the output in layers with $R(z)$ = 0 (factor 20 instead of 10 because the quantity of interest is R, which is proportional to the square of the spectrometer output). N was adjusted to make the modeled SNR for the highest value of P similar to the SNR as found during the experiments with the phantom eye, that is, a SNR of 32 dB for the high-reflective peak.

Modeling the effects of low-pass filtering of the A-scan

A (histogram-like) schematic A-scan was constructed using data from Ishikawa et al. (Fig. 2) [16] and Darma et al. (Fig. 4(C)) [2]. Table 2 shows the thickness and signal strength of the layers. The A-scan was modeled with a resolution of 0.1 µm. Low-pass filtering was modeled by convolving the schematic A-scan with a Gaussian filter. Two standard deviations were used, being σ = 5 and 10 µm, respectively. The calculations were repeated for an eye with a thinned RNFL (10 µm instead of 20 µm). All model calculations were performed using Octave (version 3.6.2; www.gnu.org/software/octave/) for Linux (Ubuntu 12.10).

Biomedical Optics EXPRESS

Table 2. Layer thickness and signal strength of the schematic A-scan

Layer	Thickness (µm)	Signal strength (dB)
vitreous		50
RNFL	20	80
RGCL	30	65
IPL	20	68
INL	30	59
OPL	20	65
ONL + IS	130	56
IS/OS	20	83
OS	20	71
RPE	30	86
choroid		65

3. Results

Figure 3 shows the measured signal strength in the phantom eye, as a function of light source power. At higher powers, the vertical distance between the traces was - as expected - approximately 6 dB. At lower powers, this distance decreased. Peak widths tended to decrease with decreasing power. For all powers, the medium- and high-reflective layers (peaks) were clearly wider and the low-reflective layers (valleys) narrower than the expected 50 µm. For the first (medium-reflective) peak, the FWHM as determined with Origin 6.0 ranged from 64 to 73 µm going from the lowest to the highest light source power; this was 84 to 97 µm for the last (high-reflective) peak.

The upper panel of Fig. 4 presents the modeled signal strength in response to a 50 µm medium-reflective layer between two low-reflective layers and a 50 µm high-reflective layer between two low-reflective layers, as a function of light source power, for a coherence length of 12 µm. In agreement with the measurements as presented in Fig. 3, the vertical distance between the traces was approximately 6 dB at higher powers and decreased at lower powers, and this effect was clearer for the medium-reflective layer than for the high-reflective layer. The lower panel of Fig. 4 gives the corresponding first derivatives.

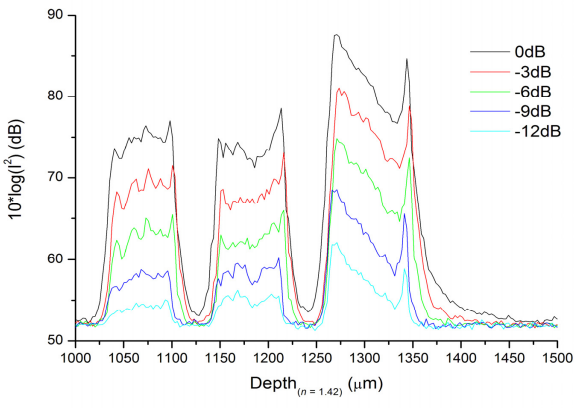

Fig. 3. Measured signal strength in the phantom eye as a function of light source power. The thickness and reflectivity of each layer is given in Table 1. The signal strength decreases with attenuation. Interestingly, the space between two reflectors seems thinner than the space inside the reflectors, even though they have the same thickness.

Biomedical Optics EXPRESS

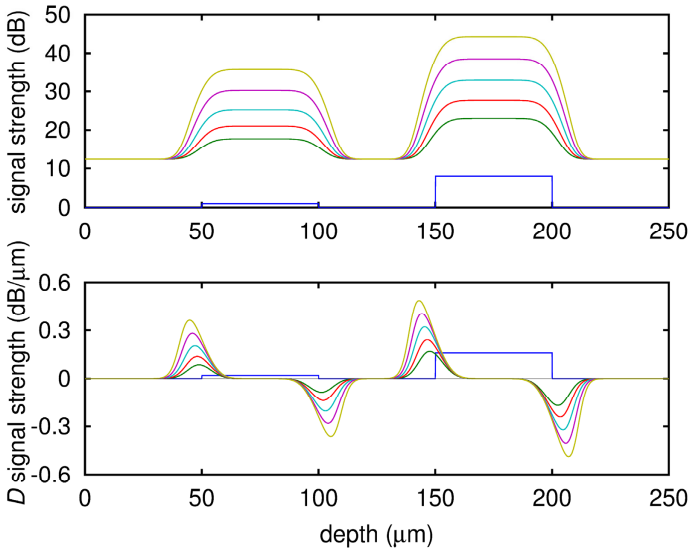

Fig. 4. Upper panel: Modeled signal strength in response to a 50 µm medium-reflective layer between two low-reflective layers and a 50 µm high-reflective layer between two low-reflective layers, as a function of light source power, for a coherence length of 12 µm. Lower panel: Corresponding first derivatives.

Table 3 shows the width of the high-reflective peak as a function of coherence length and power, with width defined as (1) FWHM (based on the upper panel of Fig. 4) and (2) the distance between the maximum and minimum of the first derivative (based on the lower panel of Fig. 4). The widths increased with increasing coherence length and power. Interestingly, the widths were larger than the underlying value of 50 µm for all coherence length and power values. Qualitatively, this agrees with the observations in the phantom eye (Fig. 3); quantitatively, the effects in the phantom eye were even somewhat more pronounced. This indicates low-pass filtering on top of the coherence function, or it might be related to the non-Gaussian shape of the coherence function [13].

Table 3. Widths of the modeled signal strength in response to a 50 µm high-reflective layer between two low-reflective layers (right peak in Fig. 4), as a function of coherence length and light source power

$P_{\text{light source}}$ (a.u.)	l_c (µm)					
	6		12		24	
	FWHM (µm)	max-min of D (µm)	FWHM (µm)	max-min of D (µm)	FWHM (µm)	max-min of D (µm)
1	52.0	52.5	53.8	54.9	57.6	59.7
2	52.8	53.5	55.4	56.9	60.6	63.9
4	53.6	54.7	57.2	59.3	64.0	68.5
8	54.6	55.9	59.0	61.7	67.4	73.2
16	55.4	57.1	61.0	64.1	70.4	77.8

FWHM = full width at half maximum of signal strength (upper panel of Fig. 4); max-min of D = distance between maximum and minimum of signal strength derivative (lower panel of Fig. 4).

Figure 5 shows the effects of low-pass filtering on a schematic A-scan profile of the human retina (blue), for Gaussian filters with 5 (green) and 10 (red) µm standard deviation.

Biomedical Optics EXPRESS

The left panel of Fig. 6 presents the inner retinal part of Fig. 5, for an intact RNFL (20 µm; upper-left panel) and a thinned RNFL (10 µm; lower-left panel); the right panel gives the corresponding first derivatives. See figure caption for a detailed description of the observed shifts of peaks and spurious thickening and thinning of layers.

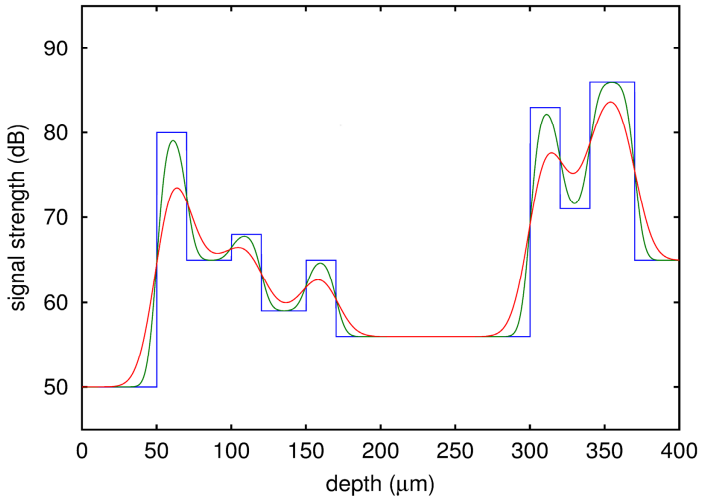

Fig. 5. Effect of low-pass filtering on a schematic A-scan profile of the whole retina (blue), for Gaussian filters with 5 (green) and 10 (red) µm standard deviation. Peaks and valleys from left to right depict the RNFL, RGCL, IPL, INL, OPL, ONL and IS, IS/OS, OS, RPE, and choroid.

4. Discussion

The inherent minimal width of the coherence length, followed by a log transform results in an overestimation of the thickness of high-reflective layers (e.g., the RNFL) and this overestimation increases with an increase in SNR. Inevitably, the thickness of a low-reflective layer sandwiched between two high-reflective layers (e.g., the RGCL) will be underestimated, and this underestimation increases with an increase in SNR. Low-pass filtering of an A-scan profile results in (1) a shift of the RNFL towards the outer retina, (2) a thickening of the RNFL, (3) a thinning of the RGCL due to the low-pass filtering itself and due to RNFL thinning – if present, (4) a shift of the IPL towards the vitreous, and (5) a thickening of the IPL. All these (illusory movement) effects increase with an increase in low-pass filtering and a (disease-induced) decrease in peak thicknesses (RNFL and IPL).

The coherence length/log transform related overestimation of the thickness of high-reflective layers cannot easily be verified in vivo, as a retina typically cannot be harvested after an OCT measurement, or is affected by shrinking and cutting artifacts in histology making such measurements hard to interpret [17]. However, an overestimation has been reported in a phantom eye, using clinically available OCT devices [1]. On average, a layer of 49 µm thickness was reported to have a thickness of 67 µm by the clinical devices. This overestimation even seems to exceed our values (Table 3), which might be caused by the fact that Kinkelder et al. used a maximized image quality, meaning that images were obtained at the highest possible SNR [1]. The authors discussed potential sources for the observed discrepancy, including inadequate dispersion compensation, a faulty *k*-calibration of the spectrometer, broadening due to a finite optical resolution, a wrong assumption regarding the refractive index, or missing knowledge on the implementation of the manufacturers' proprietary segmentation algorithm. None of these factors was identified as a likely explanation for the observed thickness overestimation. This agrees with our finding that the inherent minimal width of the coherence function and the log transform together yield a

Biomedical Optics EXPRESS

spurious thickening of peaks, where model and experiment essentially agree. A decrease in the overestimation (that is, an apparent thinning) with a decrease in SNR has been measured clinically by performing layer thickness measurements before and after a cataract extraction. Lee et al. and Mwanza et al. found with the Stratus OCT a cataract extraction induced increase in the measured thickness of the peripapillary RNFL of 5 µm and 9.3% (~9 µm), respectively [3, 4]. Nakatani et al. found a significant increase in the thickness of both the macular RGC complex (GCC; RNFL + RGCL + IPL) and the peripapillary RNFL, with the RTVue 100 [5].

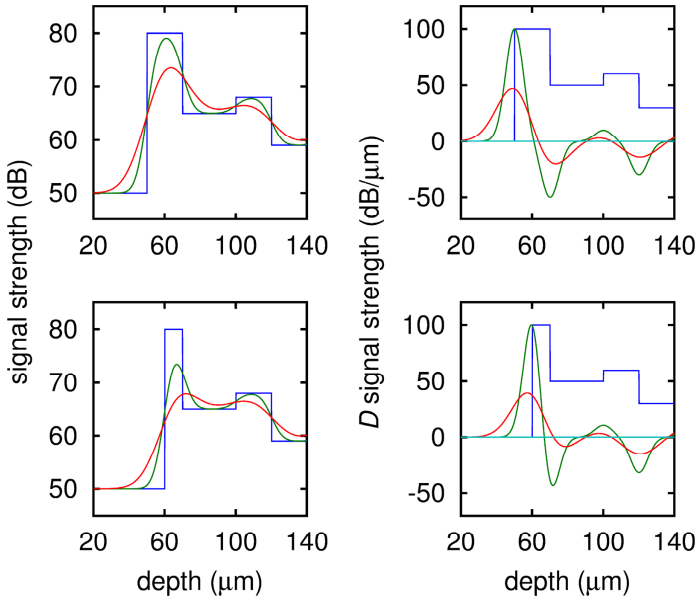

Fig. 6. Effect of thinning (upper versus lower panel) of the RNFL on the effects of low-pass filtering on a schematic A-scan profile of the inner retina (blue), for Gaussian filters with 5 (green) and 10 (red) µm standard deviation (left panel) with corresponding first derivatives (right panel). Low-pass filtering resulted in a right shift of the peak of the RNFL (upper-left panel) and - in agreement with illusory movement - this shift was more pronounced for the thinned RNFL (lower-left panel). Similarly, a left shift was observed for the IPL. If we define layer thickness using the maxima and minima of the first derivative, the RNFL thickness in the upper-right panel (unfiltered 20 µm) was 20 and 24 µm for 5 and 10 µm standard deviation, respectively, and in the lower-right panel (unfiltered 10 µm) 13 and 22 µm. The RGCL thickness (unfiltered 30 µm) in the upper-right panel was 30 and 25 µm for 5 and 10 µm standard deviation, respectively, and in the lower-right panel 28 and 19 µm. Hence, RNFL thinning causes an additional thinning of the RGCL, on top of the RGCL thinning due to the low-pass filtering itself. The IPL thickness (unfiltered 20 µm) was 20 and 23 µm for 5 and 10 µm standard deviation, respectively; independent of the RNFL thickness. The thickness of the RGC complex (RNFL + RGCL + IPL) was, for the intact RNFL, 70 and 72 µm for 5 and 10 µm standard deviation, respectively (expected thickness 70 µm) and for the thinned RNFL 61 and 64 µm (expected thickness 60 µm).

The influence of illusory movement on the accuracy of OCT measurements is difficult to weigh. Spatial low-pass filtering is part of preprocessing in segmentation algorithms, but often in an anisotropic way [8], that is, the filter width is greater parallel than perpendicular to the retinal surface. However, with a decrease in SNR the filter width in the direction of the A-scan may increase intentionally (to improve the information yield, that is, sacrificing the high spatial frequencies in order to get a more accurate estimate of the low spatial frequencies in situations with poor SNR) [18, 19] or unintentionally (for example, due to errors in the registration of adjacent A-scans or layer thickness inhomogeneities). Generally, as long as

Biomedical Optics EXPRESS

layer thickness >> filter width the effect is negligible whereas the effect becomes important as soon as layer thickness and filter width are of the same order of magnitude [9]. This implies an increase in illusory-movement artifacts with a decrease in layer thickness. We showed an underestimation of RNFL thinning and a spurious thinning of the RGCL in case of a thinning of the RNFL (Fig. 6). Darma et al. investigated the effect of a decrease in SNR, induced by using neutral density filters, on layer thicknesses as assessed with a Topcon 3D OCT (OCT-1000; Topcon Medical Systems, Tokyo, Japan) using the Iowa Reference Algorithm [20], in healthy subjects [2]. With a decrease in SNR, the most obvious changes were a thickening of the ONL + IS and a thinning of the GCC. The latter was caused by a thinning of all three contributing layers (RNFL, RGCL, and IPL). Thinning of the RNFL and IPL with decreasing SNR can easily be attributed to the coherence length/log transform issue, but the concurrent thinning of the RGCL can only be explained by an increase in low-pass filtering of the A-scan with decreasing SNR, yielding a more pronounced illusory-movement effect.

In the current manuscript, we defined layer thickness as FWHM or by detecting the layer borders using the extremes of the first derivative; for peak location we employed the zero-crossing of the first derivative. Obviously, many other approaches exist for segmenting OCT images [8]. However, the effects we describe are not caused by our assumptions. Coherence length is a fact given from physics and the log transform is a universal approach, as is low-pass filtering of the A-scan as part of preprocessing. Hence, other algorithms are not necessarily more resistant against the artifacts uncovered in this study, as they have to handle the same issues. Interestingly, as mentioned above, a spurious thickening of a high-reflective phantom eye layer has been reported for clinically available OCT devices, and a change of the RNFL thickness related to a cataract surgery induced change in SNR is a well-established clinical finding. Current device-independent segmentation algorithms like the Iowa reference algorithm [19] and the open-source algorithm of Chiu et al. [21] take the log-transformed image as starting point as well. The Iowa reference algorithm segmentation results appeared to be SNR dependent (see above). To explore the SNR dependence of the algorithm of Chiu et al., we used their Duke Optical Coherence Tomography Retinal Analysis Program (DOCTRAP software) to segment the image of Fig. 1 (upper panel, left) before and after the addition of white noise to the raw spectra that reduced the SNR of the RNFL peak from 25 to 13 dB. The RNFL thickness was 55 µm in the original image and decreased to 53 µm with the added noise – an apparently modest change (for interpretation of the thickness values, see end of Discussion section and Fig. 7).

In a recent population-based study, the mean RGCL thickness in the inferior half of a 6x6 mm macular region OCT scan ranged from 10 to 30 µm in glaucoma patients and from 20 to 40 µm in controls [22]. In that study, the mean RGCL thickness in the inferior half of the macular region scan was the best metric to discriminate between glaucoma patients and controls. The average rate of change of the peripapillar RNFL thickness was reported to be typically 1 µm/year in glaucoma patients and about half that value in controls [23–25]; similar values were found for the GCC [26]. Hence, the biases observed in the current study are at least of the same order of magnitude as clinically relevant differences between glaucoma patients and controls.

Is it possible to adjust layer thicknesses for the artifacts in order to report correct values? This is not obvious as the two main sources of errors (coherence length and illusory movement) sometimes amplify and sometimes counteract each other, and may depend on the SNR and the actual layer thicknesses. The unifying underlying problem is the log transform: not only in the coherence length/log transform issue but also for the illusory-movement phenomenon, as this phenomenon requires a low contrast between peak and flanking areas and a large contrast between the two flanking areas, and would thus be nonexistent without the log transform (see also Introduction section). The easiest way to get at least one robust and bias free thickness measure relevant to glaucoma could be to calculate the thickness of the RNFL in the raw (I^2) signal rather than using the log-transformed signal. As to be

Biomedical Optics EXPRESS

expected, for the model calculations as presented in Fig. 4 and Table 3, this resulted in bias free layer thickness estimates. However, a caveat here is that the noise within the peaks is more pronounced in the raw signal than in the log-transformed signal, which makes an accurate determination of peak height (and thus FWHM) in measured data not obvious. We analyzed the raw signal of the measurements as reported in Fig. 3. The resulting thicknesses of the peaks were thinner than those reported in the Results section for the log-transformed signal (but still somewhat thicker than expected) and essentially independent of the light source power (FWHM of the raw (I^2) signal as determined with Origin 6.0 was 65 µm for the left peak in Fig. 3 and 83 µm for the right peak, within 1 µm for all light source powers used). We also determined the FWHM of the raw signal RNFL peak in Fig. 1, before and after adding white noise to the raw spectra, providing 12 dB attenuation. This resulted in a constant thickness of 38 µm (Fig. 7, left panel). The FWHM of the RNFL peak in the log-transformed signal was 54 µm before and 43 µm adding noise (Fig. 7, right panel).

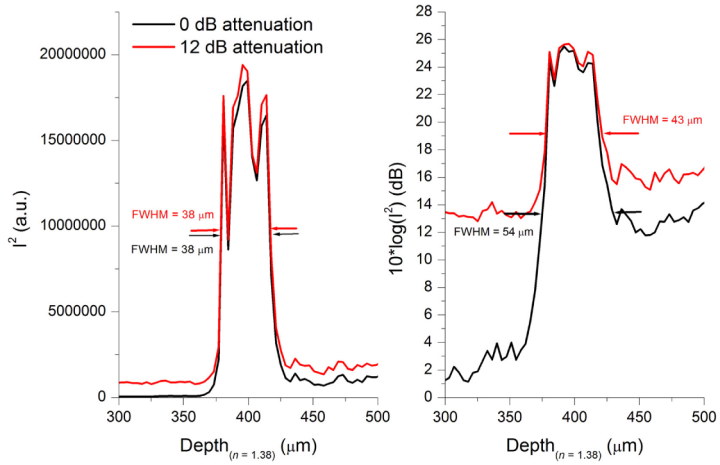

Fig. 7. RNFL peak from Fig. 1 as I^2 (left panel) and log-transformed signal (right panel), before (black line) and after (red line) adding white noise to the raw spectra, resulting in a 12 dB attenuation. FWHM values shown were determined with Origin 6.0.

5. Conclusion

In conclusion, clinically available OCT devices have sophisticated analysis tools that report layer thicknesses in a seemingly accurate way. The reported thicknesses may or may not reflect the real anatomy of the retina. Thicknesses are influenced by coherence length, the log transform, image quality (SNR), and the segmentation algorithm, and may thus differ both within and between devices. The observed biases are of the same order of magnitude as clinically relevant differences and changes and for that reason cannot be ignored. For the RNFL, the log transform related issues could possibly be circumvented by calculating its thickness as the FWHM of the raw signal, a seemingly attractive option that needs to be explored in data from glaucoma patients and healthy subjects.

Funding

Mexico's Consejo Nacional de Ciencia y Tecnologia (Conacyt; Joel Cervantes); Ministry of Education Culture, Sports, Science and Technology-Govt. of Japan (Maddipatla Reddikumar).